

Optimized Joint Time Synchronization And Channel Estimation Scheme For Block Transmission UWB Systems

SESHU KUMAR .N¹, BHARAT KUMAR SAKI², MANJULA BAMMIDI³, P SRIHARI⁴,

¹PG Student, Department Of ECE, DIET, Anakapalli, Visakhapatnam, AP, INDIA.

²PG Student, Department Of CSIT, JNTUK college of Engineering, Visakhapatnam, AP, INDIA

³Associate Professor, Department Of ECE, DIET, Anakapalli, Visakhapatnam, AP, INDIA.

⁴Associate Professor, HOD, Department Of ECE, DIET, Anakapalli, Visakhapatnam, AP, INDIA.

Abstract

In this paper, timing synchronization in high-rate ultra-wideband (UWB) block transmission systems is investigated. A new joint timing and channel estimation scheme is proposed for orthogonal frequency division multiplexing (OFDM) and single carrier block transmission with frequency domain equalization (SC-FDE) UWB systems. The scheme is based on a newly designed preamble for both coarse timing and the subsequent channel estimation. Despite of the presence of coarse timing error, the estimated channel impulse response (CIR) is simply the cyclic shifted version of the real CIR, thanks to the unique structure of the preamble. The coarse timing error (CTE) is then determined from the CIR estimation and used to fine tune the timing position and the frequency domain equalization coefficients. The proposed scheme saves preamble overhead by performing joint synchronization and channel estimation, and outperforms existing timing acquisition methods in the literature in dense multipath UWB channels. In addition, the impact of timing error on channel estimation and the performance of SC-FDE UWB systems are analyzed, and the bit-error-rate (BER) degradation with respect to certain timing error is derived.

Index Terms—Synchronization, UWB, SC-FDE, timing error analysis, joint timing and channel estimation.

I. Introduction

For high data rate ultra-wideband (UWB) communications, two block transmission systems have been proposed: orthogonal frequency division multiplexing (OFDM) [1] and single carrier with frequency domain equalization (SC-FDE) [2], both of which compare favorably to the impulse based UWB systems in terms of equalization complexity and energy collection in dense multipath UWB channels. SC-FDE has lower peak to average power ratio (PAPR) and lower sensitivity to carrier frequency offset (CFO) than OFDM, but is less robust to timing error [3]. Due to the very high data rate of UWB systems, the requirement on the

synchronization accuracy is much more stringent than conventional wideband systems. Moreover, the highly dispersive nature of UWB channels presents additional challenges to timing acquisition. The literature is abundant with research on preamble assisted synchronization methods for OFDM in conventional wideband channels [4]-[7]. Since this paper is concerned with timing synchronization,

There are only a few publications in the literature on synchronization for multi-band (MB) OFDM UWB systems [9]—[13], all using the preamble defined in the WiMedia standard [1] except [10]. Cross-correlation with the preamble template is used in [9]—[11] for synchronization, leading to high complexity. The methods in [12], [13] employ autocorrelation of the received signal as the timing metric and take the maximum of the metric to be the timing point, which tend to synchronize to the strongest path but not necessarily the first significant path. In this paper, we propose a generic joint timing and CE scheme for block transmission systems, which begins with an auto-correlation based coarse timing estimator using a newly designed preamble, followed by CE and CE assisted timing adjustment. In the coarse timing stage, the coarse FFT window position is established and the initial CE is performed. The particular preamble structure makes the CE robust to the coarse timing error, and the proposed technique to accurately estimate the coarse timing error allows both fine timing adjustment and CIR adjustment for later data demodulation. Both synchronization and CE are acquired from the procedure. This design saves the preamble overhead and improves the synchronization performance in UWB channels.

The fine timing estimation is related to the time of arrival (ToA) estimation. For ToA estimation in MB-OFDM UWB systems, energy detectors can be found in [14], [15], and an energy jump detector has been proposed in [16]. In this work, we propose a newly designed energy jump detector and provide its performance analysis. In addition, the impact of timing error on SC-FDE systems has been analyzed in this work, which is not available in the literature. The remainder of the paper is organized as follows.

Section II presents the system model and the synchronization problem formulation. The proposed timing and CE scheme is introduced in Section III. The timing error impact on SC-FDE systems with minimum mean square error frequency domain equalization (MMSE-FDE) is analyzed in Section IV. Section V gives the performance evaluation and discussion of the proposed method in UWB channels. Finally Section VI concludes the paper.

II. System Model

Although the system model adopts cyclic prefixed single carrier block transmission with frequency domain equalization over UWB channels, the synchronization technique developed directly applies to an OFDM system. The p th transmitted block is composed of digitally modulated symbols x_{pk} ($0 \leq k \leq N-1$), where N is the block length. A cyclic prefix of length N_g is used to avoid IBI as in an OFDM system. Denote the symbol-spaced equivalent CIR by $h = [h_0, h_1, \dots, h_L]$, where L is the maximum channel delay. The UWB channel is assumed to be constant over the data blocks. As long as the maximum channel delay is shorter than the CP length ($L < N_g$), there is no FBI in data demodulation with perfect timing. The task of synchronization is to find the beginning of the data block, also referred to as finding the FFT window position. Perfect synchronization in cyclic prefixed block transmission systems can be achieved in the IBI-free region of the CP ($[-N_g+L, 0]$) [5]. As long as the FFT window starts within the IBI-free region, data demodulation can be carried out perfectly. Otherwise timing error will cause performance degradation to a system. In Section IV, the effect of timing offset on the performance of SC-FDE UWB will be analyzed

III. The Proposed Joint Timing and Channel Estimation Scheme

Timing within the IBI-free region does not cause extra interference to the detection. However, in UWB systems, the IBI-free interval given a short CP is often very small or even zero, depending on channel realizations. Thus, it is necessary to locate the first significant arrival path of the transmitted signal block, which is defined as the exact timing point in the following. With the definition of the exact timing point, we define the timing error as the offset between the established timing point and the exact timing point.

A. Preamble Structure and Coarse Timing

In dense multipath channels, coarse timing obtained by evaluating a metric function can not provide sufficient accuracy, since coarse timing often falls far away from the exact timing due to the large channel dispersion. We propose to use the estimated channel information to fine tune the timing position. A new preamble structure is designed to have the periodical property for acquisition and cyclic

structure for accurate CE whose result will be used in the subsequent timing adjustment and frequency domain equalization. As shown in Fig. 1, in addition to the CP, a cyclic suffix is padded after the preamble body. Note that the suffix is used only for the preamble, and data blocks have CP only as in conventional OFDM. In the proposed preamble shown in Fig. 1, A and B represent the first half and the second half of one block generated by

$$P_t^{(n)} = \frac{1}{\sqrt{N}} \sum_{k=0}^{N-1} P_t(k) e^{j2\pi nk/N} \quad 0 \leq k \leq N-1 \quad (1)$$

where $P_t(k)$ is a random ± 1 sequence in frequency domain (FD), referred to as FD pilot block, which results in flat amplitude in FD for good CE performance. The [A B] structure can be repeated M times and finally a prefix and a suffix are added to have [B A B ... B A], where A and B are the first N_x samples of A and last N_x samples of B respectively. The length of the prefix and suffix denoted by N_x needs to be larger than the maximum coarse timing error, and N_x should be larger than the channel length L to avoid IBI. By repeating [A B] we can achieve noise averaging for more accurate CE, and the adjacent [A B] blocks serve as cyclic extension. For the case of $M=1$, the whole preamble becomes [B A B A], thus the synchronization and CE overhead is $2N_x+N$, smaller than the preamble pattern proposed in [1] where the overhead is $2(N+N_g)$. Following the conventional auto-correlation based metric function, we define our timing metric function as

$$M(d) = \frac{2|C(d)|}{R(d)} = \frac{2 \left| \sum_{k=0}^{2N_x+(M-1)N-1} r_{d+x}^x r_{d+N+1} \right|}{\sum_{k=0}^{2N_x+(M-1)N-1} (|r_{d+1}|^2 + |r_{d+N+1}|^2)} \quad (2)$$

and coarse timing is established by finding the maximum of (2) as given by $6C = \max M(d)$. Note the range of d to look for the maximal can be defined as $[9S, 9S + Q]$, where $6S$ is the point where the metric function first exceeds the preset threshold and Q can be set as N . Simply speaking, the metric calculator activates the maximization procedure once the arrival of the signal is sensed. To reduce the computation complexity at the implementation stage, the metric can be implemented in an iterative manner similar to [4] as

$$C(d+1) = C(d) - r_d r_{d+N} + r_{d+2N_x+(M-1)N} r_{d+2N_x+MN} \quad (3) \quad \text{and}$$

$$R(d+1) = R(d) - |rd|^2 - |rd+N|^2 + |r_{d+2N_x+(M-1)N}|^2 + |r_{d+2N_x+MN}|^2 \quad (4)$$

which implies a sliding window implementation. For every received sample, only 3 new multiplication and

6 add operations are needed to compute the iterative timing metric. This sliding window correlator saves substantial complexity compared to the metrics proposed in [7] and [9] which need to perform the whole correlation for every received sample.

B. Channel Estimation and Timing Adjustment

In this step, CE is carried out using the same preamble after the initial acquisition and the estimation accuracy is not affected by the timing error. Denote the coarse timing error (CTE) by ϵ_c number of symbols. Consider the low complexity least square (LS) CE. If $M = 1$, the frequency domain CE is given by $H(k) = \frac{1}{N} \sum_{l=0}^{N-1} g(l) e^{j2\pi k l / N}$, where $P_r(k)$ and $P_t(k)$ denote the received and transmitted frequency domain training symbol at the A :th subchannel respectively. The estimation can be improved by employing the repetitive $[A \ B]$ structure to reduce the noise effect. In addition, the cyclic structure given by B and A provides IBI-free CE as long as the coarse timing error $|\epsilon_c| < N_x$. In this case, the estimated channel is given by

$$H_k = H_k e^{2\pi j \epsilon_c k / N} + W_k \quad (5)$$

where W_k is the Gaussian noise in frequency domain.

Since the proposed preamble has a cyclic structure, the estimated frequency domain channel using this preamble does not suffer from the coarse timing error induced IBI that is usually present in conventional schemes. The impact of coarse timing error on the CE with conventional preambles will be shown in Section IV-C. Performing inverse FFT (IFFT) on H_k , the estimated CIR g is the CIR h cyclicly shifted by the timing error of ϵ_c samples, plus the Gaussian noise. The CTE ϵ_c can be estimated from g and then used to adjust timing for the subsequent data blocks, which has no cyclic property to use as the preamble does. The coarse timing error estimation is obtained by an energy jump detector written as

$$\epsilon_c = \begin{cases} -T_0 & \text{if } 0 \leq T_0 < \frac{N}{2} \\ N - T_0 & \text{if } \frac{N}{2} \leq T_0 < N \end{cases} \quad (6)$$

where

$$T_0 = \max_{0 \leq i \leq N-1} E(i) \quad (7)$$

$$E(i) = \begin{cases} e_r(i) - e_l(i) & \text{if } |g_i| < n |g_{\max}| \\ e_r(i) + e_l(i) & \text{if } |g_i| \geq n |g_{\max}| \end{cases} \quad (8)$$

$$\text{and } e_r(i) = \sum_{k=0}^{\epsilon-1} |g(i+k) \bmod N|^2$$

$$e_l(i) = \sum_{k=0}^{\epsilon-1} |g(i-k-1) \bmod N|^2 \quad (9)$$

Where (g_{\max}) is the maximum absolute value of the elements in g and T is a preset threshold whose determination will be given in Section V. Fig. 2 is an example of g obtained by simulation using the CM2 channel model. In this example, the block length is $N = 128$. Due to the coarse timing error, the actual CIR is cyclic shifted, and thus some strong taps at the end of the vector g are observed which correspond to the channel taps shifted. The first significant tap is near the end of the vector g , meaning that the current timing is several samples to the right of the exact timing point. The first tap of g can be determined by (6)-(9) and explained as follows. Once an estimated channel tap $g(i)$ is above a normalized threshold $\frac{1}{75} g_{\max}$ the energy of f channel taps on the right side of i represented by $e_r(i)$ is compared to the energy of ℓ channel taps on the left side of i represented by $e_l(i)$, to evaluate the energy jump on the point i . The first channel tap to be detected at the position where the energy jump is the largest. Having a window of ℓ channel taps is to reduce the occurrence of mistakenly choosing a noise tap as the first tap. Since before the first tap there are only noise, whereas $e_r(i)$ contains energy from the channel taps and noise, $e_r(i) - e_l(i)$ cancels the noise and can well detect the jump point from the noise only region to the starting of the CIR g . The determination of parameters i and ℓ will be discussed in Section V. Upon obtaining the coarse timing error, the synchronizer can adjust timing position by ϵ_c samples, and at the same time, the CE result should also be modified corresponding to the timing adjustment by $H^k = H_k e^{2\pi j \epsilon_c k / N}$. Note that in (6), we determine the timing error to the left or right of the exact timing by the search result being in the first half or the second half of the CIR. Therefore, the

fine timing can handle at most $\frac{N}{2}$ coarse timing

error, which is usually more than sufficient. The block diagram of the entire timing synchronizer for SC-FDE UWB systems is shown in Fig. 3. When the timing metric module detects the coarse timing point, it passes the received signal to the subsequent modules. The LS estimator estimates FD channel response H_k based on the coarse FFT window, and then the coarse timing error is estimated by the CTE estimator based on the coarse CE result. Finally the CTE estimation is used to adjust the FFT window position and the FDE channel coefficients.

C. Performance of Fine Timing Adjustment

The performance of the fine timing adjustment is solely dependent on the accuracy of the

first tap search, given a set of estimated channel taps. The conventional energy detector [6], [14], [15] usually measures the energy in a window of channel taps and takes the starting point of the maximal measurement window as the first tap position. However, this method requires the knowledge of the exact channel length, which is usually difficult to estimate accurately in UWB channels. Setting the window too long may lead to an early timing while having the window too short may lead to a late timing. The proposed energy jump detector overcomes this drawback of the conventional energy detector. Its window length does not need to equal the exact channel length and usually a window length less than the channel length is sufficient. With a moderate window length, the energy jump detector can achieve accurate timing. Note that another energy jump detector has been proposed in [16], where the metric is in an energy ratio form while that of the proposed detector is in a subtraction form. The detector in [16] is able to deal with the more realistic channel with continuously varying delays at the cost of higher complexity. That is, CIR is estimated more frequently in [16]. In the following, we study the timing error probability of the proposed energy jump detector in comparison with that of the conventional energy detector. The energy jump factor at the exact timing point d can be written as

$$E(d) = \sum_{k=0}^{\varepsilon-1} |g(d+k) \bmod N|^2 - \sum_{k=0}^{\varepsilon-1} |g(d-k-1) \bmod N|^2$$

$$= \sum_{k=0}^{\varepsilon-1} (|h_k + \omega(d+k) \bmod N|^2 - |\omega(d-k-1) \bmod N|^2) \quad (10)$$

where W_k is the noise component of the k th element of the estimated CIR vector. We study the case where the window length is less than the channel length ($\varepsilon < L$), usually resulting in late timing with the conventional energy detector. For the case of $\varepsilon > L$, the analysis is similar.

Consider a late timing event of t samples where $t > 0$. For the conventional energy detector, the error probability that a late timing of t samples occurs is given by

$$P_{ED}(t) = \Pr \left(\sum_{k=0}^{t-1} |h_k + \omega(d+k) \bmod N|^2 < \sum_{k=0}^{t-1} (|h_{\varepsilon+k} + \omega(d+\varepsilon+k) \bmod N|^2) \right) \dots (11)$$

Following [15], we consider the complex Gaussian channel taps with variances decaying along the index. Assume the small number of t adjacent channel taps on the right side of (11) have the same

variance $\sigma \frac{2}{1}$. Similarly, the t adjacent taps on the left side of (11) have approximately equal variance denoted by $\sigma \frac{2}{w}$. Then both sides of (11) are scaled Chi-square distributed random variables (r.v.s) with $2t$ degrees of freedom and the component Gaussian's variance $\sigma \frac{2}{1} + \sigma \frac{2}{w}$ and $\sigma \frac{2}{2} + \sigma \frac{2}{w}$ respectively, where $\sigma \frac{2}{w}$ is the variance of the noise component in the coarse CE result. Then the probability in (11) can be written as

$$P_{ED}(t) = \int_0^\infty f_l(x) \int_z^\infty f_r(y) dy dx \quad (12)$$

where $f_l(x)$ and $f_r(x)$ represent the probability density function (PDF) of the left side and right side of (11) respectively. The PDF of a scaled Chi-square r.v. of $2t$ degrees of freedom is $f(x) = \frac{1}{\sigma^{2\varepsilon} 2^t \Gamma(t)} x^{t-1} e^{-x/2\sigma^2}$, where σ^2 is the component Gaussian's variance. Substituting the PDF of the Chi-square r.v. into (12), the error probability can be written as

$$P_{ED}(t) = \frac{1}{r(t)} \sum_{k=0}^{t-1} \frac{1}{k!} \frac{\left(\frac{\sigma_1^2 + \sigma_w^2}{\sigma_1^2 + \sigma_w^2} \right)^{t+k} \Gamma(t+k)}{\left(1 + \frac{\sigma_1^2 + \sigma_w^2}{\sigma_1^2 + \sigma_w^2} \right)^{t+k}} \Gamma(t+k) = \frac{1}{r(t)} \sum_{k=0}^{t-1} \frac{1}{k!} \frac{\gamma_0^k}{(1 + \gamma_0)^{t+k}} \Gamma(t+k) \quad (13)$$

where $\Gamma(\cdot)$ is the Gamma function with $\Gamma(k) = (k-1)!$ and $\gamma_0 = \frac{\sigma_1^2 + \sigma_w^2}{\sigma_1^2 + \sigma_w^2}$. Indeed 70

represents the energy ratio of the estimated channel tap (including noise) at the actual first channel tap position over that at the $+1$ actual tap position. This definition takes into account the power decaying over time.

For the proposed energy jump detector, the event of timing error of t samples happens when $E(d) < E(d+t)$. Similar to (10),

$$E(d+t) = \sum_{k=0}^{\varepsilon-1} |g(d+t+k) \bmod N|^2 \sum_{k=0}^{\varepsilon-1} |g(d+t-k-1) \bmod N|^2$$

$$= \sum_{k=0}^{\varepsilon-1} |h_{k+t} + \omega(d+k+t) \bmod N|^2$$

$$\sum_{k=0}^{\varepsilon-1-t} |\omega(d-k-1) \bmod N|^2 - \sum_{k=0}^{t-1} |h_k + \omega(d+k) \bmod N|^2.$$

(14)

Then the probability of the event for the proposed energy jump detector can be written as'

$$P_{EJ}(t) = \Pr(E(d) < E(d+t)) = \Pr\left(2 \sum_{k=0}^{t-1} |h_k + \omega(d+k) \bmod N|^2\right) < \sum_{k=0}^{t-1} (|h_{\varepsilon} + \omega(d+\varepsilon+k)|^2 + |\omega(d-\varepsilon+k) \bmod N|^2).$$

(15)

The left side of (15) is a scaled Chi-Square r.v. with 2t degrees of freedom and the component Gaussian's variance $2(\sigma \frac{2}{1} + \sigma \frac{2}{w})$, while the right side of (15) is a sum of two scaled Chi-Square random variables with It degrees of freedom and the component Gaussian's variances $\sigma \frac{2}{3} + \sigma \frac{2}{w}$ and $\sigma \frac{2}{w}$. Then the timing error probability can be written as:

$$P_{EJ}(t) = \int_0^{\infty} f_1(x) \int_x^{\infty} f_r(y) dy dx = \int_0^{\infty} f_L(x) \dot{Y}(x) dx$$

(16)

Where $\dot{Y}(x) = \int_x^{\infty} \int_T(y) dy$. According to [17], $\dot{Y}(x)$ can be written as

$$\dot{Y}(x) = \sum_{k=1}^2 \sum_{t=1}^t \frac{\Theta_{k,t}(-\beta_k)}{(t-1)! \beta_k^{t-1}} \sum_{i=0}^{t-1} \frac{(\beta_k x)^i e^{-\beta_k x}}{i!}$$

(17)

Where

$$\beta_1 \equiv \frac{1}{2(\sigma_2^2 + \sigma_\omega^2)}$$

(18)

$$\beta_2 \equiv \frac{1}{2\sigma_\omega^2}$$

(19)

$$\Theta_{1,t}(t) \equiv (-1)^{t-1} \frac{(t+l-2)!}{(t-1)! (\beta_2 - \beta_1)^{t+l-1}}$$

(20)

$$\Theta_{2,t}(t) \equiv (-1)^{t-1} \frac{(t+l-2)!}{(t-1)! (\beta_1 - \beta_2)^{t+l-1}}$$

(21)

Defining $\beta_0 = \frac{1}{4(\sigma_1^2 + \sigma_\omega^2)}$, and substituting (17) and the PDF of the Chi-square r.v. into (16), we have

$$P_{EJ}(t) = \frac{\beta_0^t \beta_1^t \beta_2^t}{\Gamma(t)} \sum_{k=1}^2 \sum_{l=1}^t \sum_{i=0}^{t-1} \frac{\Theta_{k,l}(-\beta_k) \beta_k^{i+l-t-1}}{i!(l-1)!} \int_0^{\infty} \chi^{i+t-1} e^{-(\beta_0 + \beta_k)x} dx$$

$$= \frac{\beta_0^t \beta_1^t \beta_2^t}{\Gamma(t)} \sum_{k=1}^2 \sum_{l=1}^t \sum_{i=0}^{t-1} \frac{\Theta_{k,l}(-\beta_k) \beta_k^{i+l-t-1} \Gamma(i+t)}{i!(l-1)! (\beta_0 + \beta_k)^{i+t}} = \frac{1}{\Gamma(t)} \sum_{l=1}^t \sum_{i=0}^{t-1} \frac{(-1)^{l-1} (t+l-2)! \Gamma(i+t)}{(t-1)! i!(l-1)!} \left(\frac{\gamma_1^{i+l-1} \gamma_2^t}{(\gamma_2 - \gamma_1)^{i+l-1} (1 + \gamma_1)^{i+t}} + \frac{\gamma_2^{i+l-1} \gamma_1^t}{(\gamma_1 - \gamma_2)^{i+l-1} (1 + \gamma_2)^{i+t}} \right)$$

(22)

The energy ratios defined by are related to the signal-to-noise-ratio (SNR) and the UWB channel statistics, and they determine the performance of the estimator. Fig. 4 shows the timing error probability comparison of the proposed energy jump detector and the conventional energy detector with specific energy ratios. In the proposed energy jump detector, the first channel tap searching algorithm has slightly higher computation complexity than the conventional energy detector. It requires calculating the energy of two windows and performing a subtraction while the conventional detector only computes one. However, the window in the energy jump detector is usually shorter than the channel-long window of the conventional energy detector.

IV. The Impact of Timing Error on the SC-FDE Performance

The timing error impact on a general OFDM system and on an MB-OFDM system was

analyzed in [18] and [19] respectively. However, the timing error impact on SC-FDE UWB systems has not been well studied. The sub-symbol level timing offset analysis and timing jitter analysis on SC-FDE UWB systems were studied in [3], where it was shown that the sub-symbol level timing offset determines the sampling position of the equivalent channel and even the worst sub-symbol level timing offset only results in small performance degradation. Timing jitter was found to be more detrimental to system performance. Here, we study the symbol level timing offset which will be shown to have more adverse effect than sub-symbol level timing offset.

A. Small Delay Spread Channels

Small delay spread channels refer to channels with the maximum delay shorter than CP, i.e. $N_g > L$. Let m denote the timing error, and assume $|m| < N_g - L$. When $m < 0$, the starting point of the established FFT window falls in the IBI-free part of CP, leading to the same performance as that of the exact timing point. However, when $m > 0$, the established FFT window is on the right of the correct window, meaning that the current block window contains m samples of the next block. Assuming carrier frequency is perfectly synchronized, the p th received block as shown in Appendix I can be written as

$$Y(P) = \bar{h}_1^m \bar{x}_1^m(p) + n \quad (23)$$

where h is the Toeplitz channel matrix with $[h_0 \ 0 \dots 0 \ h_L \ h_{L-1} \dots h_1]_{1 \times N}$ as its first row. $x_m(p)$ is the $N \times 1$ desired p th data block left cyclic shifted by m (> 0), n is the Gaussian noise,

$$x^m(p) = \begin{bmatrix} 0, \dots, 0, x_{p+1, -N_g} - T_p, 0, x_{p+1, -N_g+1} - T_{p,1}, \dots, \\ x_{p+1, -N_g+m-1} - X_{p,m-1} \end{bmatrix}_{N \times 1}^T \quad (24)$$

where x_{pn} denotes the n th ($-N_g < n < N - 1$) symbol in the p th block, and

$$\bar{h}_1^m = \begin{bmatrix} 0_{(N-m) \times (N-m)} & h_0 & 0 & \dots & 0 \\ 0_{(N-m) \times (N-m)} & h_1 & h_0 & \dots & 0 \\ 0_{m \times (N-m)} & \vdots & \vdots & \ddots & \vdots \\ h_{m-1} & \dots & h_0 & & \end{bmatrix}$$

The received block in (23) can be seen as the combination of two convolutions plus the AWGN: one is the circulant convolution between $x^m(p)$ and the channel h , and the other one is the linear convolution between h and $x_y(p)$. After FFT, FDE,

and BFFT, the demodulated block can be written as

$$x(p) = F^H C A F x^m(p) + F^H C F \bar{h}_1^m(p) + C F_n \quad (26)$$

Where F and F^H are the $N \times N$ FFT and IFFT operation matrices respectively, and A is diagonal representing the estimated frequency domain channel response. In the presence of timing offset, the quality of CE is degraded as will be shown in Section IV-C. However, employing our proposed preamble and the joint timing and CE algorithm in Section m, the effect of timing offset on CE is only a phase shift in the frequency domain. Therefore, $H_k = H_k e^{j2\pi m(n-i)/N}$ ignoring the noise effect, where the phase shift is directly included in the CE. Let $*1 > m = F^H C F h_y$ and the (e, n) th (the matrix index starts from 0) element of $*1^m$ is given by

$$\Psi_{k,n}^{1,m} = \begin{cases} 0 & n < N - m \\ \frac{1}{N} \sum_{i=0}^{N-1} \sum_{k=0}^{N-1} C_i h_{t-n} \varepsilon^{j \frac{2\pi m(m-t+h)}{N}} & N - m \leq n \leq N - 1 \end{cases} \quad (27)$$

Then the demodulated block can be rewritten as

$$x(p) = \frac{1}{N} \sum_{k=0}^{N-1} \mu_k x(p) + I_{isi} + \Psi^{1,m} \bar{x}_1^m(p) + \bar{n} \quad (28)$$

Where $\mu_k = \frac{|H_k|^2}{|H_k|^2 + N_0 / (2E_h)}$, I_{isi} is the inter-symbol interference from the current block due to the fact that an MMSE receiver is not inter-symbol interference (ISI) free [2], and n is the Gaussian noise term with variance

$$\sigma_n^2 = \frac{N_0}{2N^2} \sum_{l=0}^{N-1} \left| \sum_{k=0}^{N-1} C_k e^{-\frac{j2\pi l k}{N}} \right|^2$$

The i th element of I_{isi} is $\sum_{\substack{n=0 \\ n \neq i}}^{N-1} S_n(i) x_{p,n}$ Where

$$S_n(i) = \frac{1}{N} \sum_{k=0}^{N-1} \mu_k e^{-j2\pi(n-i)k/N}$$

The third term in (28) is the timing error induced interference. Define the index set $[0, N-1]$ as U and the subset $[0, m-1]$ as $U \setminus$. Then for $i \in U \setminus$, the demodulated symbol can be written as

$$x_{pmi} = \left(\frac{1}{N} \sum_{k=0}^{N-1} \mu_k - \Psi_{i, N-m+i}^{1,m} \right) x_{p,i}$$

$$\begin{aligned}
 & + \overbrace{\sum_{n=m}^{N-1} S_n(i)x_{p,n} + \sum_{\substack{n=0 \\ n \neq i}}^{m-1} (S_n(i) - \Psi_{i, N-m+n}^{I,m})x_{p,n}}^{\text{in-block ISI}} + \\
 & \underbrace{\sum_{n=0}^{m-1} \Psi_{i, N-m+n}^{I,m} x_{p+1, -N_9 + n + n_{ij}}}_{\text{IBI}} \\
 & \quad (29)
 \end{aligned}$$

and for $i \in U/U_1$, the demodulated symbol can be written as

$$\begin{aligned}
 x_{p,i} &= \frac{1}{N} \sum_{k=0}^{N-1} \mu_k x_{p,i} + \underbrace{\sum_{n=0}^{m-1} \Psi_{i, N-m+n}^{I,m} x_{p+1, -N_g + n}}_{\text{IBI}} \\
 & + \overbrace{\sum_{n=m}^{N-1} S_n(i)x_{p,n} + \sum_{n=0}^{m-1} (S_n(i) - \Psi_{i, N-m+n}^{I,m})x_{p,n}}^{\text{in-block ISI}} + \bar{n}_i \\
 & \quad (30)
 \end{aligned}$$

The interference includes the in-block ISI which comes from the current block and the IBI coming from the succeeding block. There are a large number of independent interference symbols in (29) and (30), therefore Gaussian approximation can be applied to the sum of ISI according to the Lyapunov's central limit theorem as shown in the Appendix B. The variance of the interference for the z th desired symbol is denoted by $\sigma_s^2(i)$ which can be written as

$$\begin{aligned}
 \sigma_s^2(i) &= \sum_{n=m}^{N-1} |S_n(i)|^2 + \sum_{\substack{n=0 \\ n \neq i}}^{m-1} |S_n(i) - \Psi_{i, N-m+n}^{I,m}|^2 \\
 & + \sum_{n=0}^{m-1} |\Psi_{i, N-m+n}^{I,m}|^2. \quad (31)
 \end{aligned}$$

Without loss of generality, considering the BPSK symbols, the bit error rate (BER) is given by $P_e(x_{p,i}) = P(5R\{\mathcal{R}\Psi_{i, N-m+i}\} > 0 | x_{p,i} = -1)$. Therefore, the error probability is given by

$$P_e(x_{p,i}) = Q \left(\frac{\sum_{k=0}^{N-1} p_k - \Re(\Psi_{i, N-m+i}^{I,m})}{N \sqrt{\sigma_s^2(i) + \frac{\sigma_n^2}{E_b}}} \right), i \in U_1 \quad (32)$$

$$P_e(x_{p,i}) = Q \left(\frac{\sum_{k=0}^{N-1} \mu_k}{N \sqrt{\sigma_s^2(i) + \frac{\sigma_n^2}{E_b}}} \right), i \in U/U_1 \quad (33)$$

where $5R\{-\}$ is taking the real part of a complex number. Then the overall average BER can be

$$\text{obtained by } \bar{P}_e = \frac{1}{N} \sum_{i=0}^{N-1} P_e(x_{p,i}).$$

B. Large Delay Spread Channels

In the large delay spread channels, there is often no IBI-free region within the CP, and hence timing error on both sides of the exact timing point may cause performance degradation. When $m > 0$, the established EFT window contains multipath components from both the previous and the next block. Considering the case when timing error is small, i.e., $m < L - N_g$, and letting $v = L - N_g - m$, the demodulated block can be written as

$$\bar{x}(p) = F^H C A F_{x^m}(p) + F^H C F \left(\bar{h}_1^m \bar{x}(p) \right) + F^H C F_n \quad (34)$$

Where $\bar{x}_2^v(p)$ and \bar{h}_2^v are given by

$$\begin{aligned}
 \bar{x}_2^v(p) &= [x_{p-1, N-v} - x_{p, N-L, x_{p-1, N-v+1}} - x_{p, N-L+1}, \\
 & \dots, x_{p-1, N-1} - x_{p, N-N_g-1}, \underbrace{0, \dots, 0}_{N-v}]^T N_x 1 \quad (35)
 \end{aligned}$$

$$\bar{h}_2^v = \begin{bmatrix} h_{L-1} & h_{L-2} & \dots & h_L \\ 0 & h_{L-1} & \dots & h_{L-v+1} & 0_{v \times (N-v)} \\ 0 & 0 & \ddots & \vdots & \\ 0 & 0_{(N-v) \times v} & \dots & h_{L-1} & 0_{(N-v) \times (N-v)} \end{bmatrix} \quad (36)$$

The IBI has contribution from the preceding block and the succeeding block. Note that $\bar{h}_1^m \bar{x}_2^v(p) = \bar{h}_2^v \bar{x}_1^m(p) = 0$, and then (34) can be rewritten as

$$\begin{aligned}
 \bar{x}(p) &= F^H C A F_{x^m}(p) + F^H C F \left(\bar{h}_1^m + \bar{h}_2^v \right) \left(\bar{x}_1^m(p) + \bar{x}_2^v(p) \right) \\
 & + F^H C F_n \quad (37)
 \end{aligned}$$

Let $\Psi^{2,m,v} = F^H C F \left(\bar{h}_1^m + \bar{h}_2^v \right)$ and define the index subsets $U_2 = [0, m, -1]$ and $U_3 = [N - L + v, N - N_g]$. Following the same procedure in the previous subsection, the variance of the interference can be obtained as

$$\sigma_s^2(i) = \sum_{\substack{n \in U_z \\ n \neq i}} |S_n(i) - \Psi_{i, N-m+i}^{2,m,\nu}|^2 + \sum_{\substack{n \in U_z \\ n \neq i}} |S_n(i) - \Psi_{i, N+L-m}^{2,m,\nu}|^2 + \sum_{\substack{n \in U_2 \cup U \\ n \neq i}} |S_n(i)|^2 + \sum_{n \in U \cup U_3} |\Psi_{i,n}^{2,m,\nu}|^2. \quad (38)$$

For large timing error $m > L - N_g > 0$, the problem becomes the same as Subsection IV-A. Then the error probability of the i th symbol of the p th block is given by

$$P_\varepsilon(x_{p,i}) = Q \left(\frac{\sum_{k=0}^{N-1} \mu_k - \Re(\Psi_{i, N-m+1}^{2,\nu})}{N \sqrt{\sigma_s^2(i) + \frac{\sigma_\varepsilon^2}{E_k}}} \right), i \in U_2 \quad (39)$$

$$P_\varepsilon(x_{p,i}) = Q \left(\frac{\sum_{k=0}^{N-1} \mu_k - \Re(\Psi_{i, i+L-N}^{2,m,\nu})}{N \sqrt{\sigma_s^2(i) + \frac{\sigma_\varepsilon^2}{E_k}}} \right), i \in U_3 \quad (40)$$

$$P_\varepsilon(x_{p,i}) = Q \left(\frac{\sum_{k=0}^{N-1} \mu_k}{N \sqrt{\sigma_s^2(i) + \frac{\sigma_\varepsilon^2}{E_k}}} \right), i \in (U - U_2 \cup U_3). \quad (41)$$

When the timing point is to the left of the exact timing point, i.e., $m < 0$, the interference comes only from the previous block, and the demodulated block is given by

$$\bar{x}(p) = F^H C A F x^m(p) + F^H C F_h^- \bar{x}_2^\nu(p) + F^H C F n \quad (42)$$

where $\nu > L - N_g$, resulting in more multipath components from the previous block. The variance of the interference can be written as

$$\sigma_\varepsilon^2(i) = \sum_{\substack{n \in U \\ n \neq i}} |S_n(i) - \Psi_{i, n-N+L-m}^{3,\nu}|^2 + \sum_{\substack{n \in U_4 \\ n \neq i}} |S_n(i)|^2 + \sum_{n=0}^{\nu-1} |\Psi_{i,n}^{3,\nu}|^2 \quad (43)$$

where $\Psi^{3,\nu} = F^H C F \bar{h}_2^\nu$ and U_4 is defined as $[N - N_g - \nu, N - N_g]$. Thus, the i th symbol error probability can be derived as

$$P_\varepsilon(x_{p,i}) = Q \left(\frac{\sum_{k=0}^{N-1} \mu_k - \Re(\Psi_{i, i+N+L-m}^{3,m,\nu})}{N \sqrt{\sigma_s^2(i) + \frac{\sigma_\varepsilon^2}{E_b}}} \right), i \in U_4 \quad (44)$$

$$P_\varepsilon(x_{p,i}) = Q \left(\frac{\sum_{k=0}^{N-1} \mu_k - \Re}{N \sqrt{\sigma_s^2(i) + \frac{\sigma_n^2}{E_b}}} \right), i \in U \text{ and } i \in U_4. \quad (45)$$

C. The Impact of Timing Error on Channel Estimation

In the literature, CE and synchronization often employ separate preamble blocks instead of the single preamble proposed in Section IE, for example in the Multi-band OFDM standard proposal [1]. Conventional preambles usually begin with synchronization blocks, followed by CE pilot blocks and then data symbols. This subsection considers timing error induced degradation in CE with conventional preamble blocks. Note that channel estimation in SC-FDE is identical to OFDM. Consider the least square CE with one pilot block p^* . Under a timing error of $m (> 0)$ samples, the frequency domain received pilot block can be written as

$$P_r(m) = \Lambda \Omega(m) P_t + F \bar{h}_1^m \bar{P}_t^m + \bar{n}. \quad (46)$$

where Ω and P_t are diagonal matrix with elements $e^{j2\pi km} / N$ and the frequency domain pilot block respectively, is defined as

$$\begin{bmatrix} 0, \dots, 0, x_0, -N_g - p_t, 0, \dots, x_0, -N_g + 1 - p_t, \dots, x_0, N_g + m - p_t, \dots \end{bmatrix}_{N \times 1}^T$$

where x_0 is the data block following the pilot block.

Define $\Phi_{(N \times m)}^+$ as the last m columns of the matrix

$F_{h_1}^{-m}$, and its (k, n) th element is given by

$$\Phi_{k,n}^+(m) = \sum_{l=0}^{m-n} h_l e^{-j2\pi k(n-m)/N}, \quad m > 0. \quad (47)$$

Then the f th sub-carrier of P_r can be written as

$$P_r(k/m) = H_k e^{j2\pi km} / N P_t(k) + \sum_{n=0}^{m-1} \Phi_{k,n}^+(x_{0,n} - p_{t,n}) + \bar{n}_k, \quad (48)$$

The estimated channel at the kth sub-carrier is

$$H_k = \frac{P_r(k/m)}{P_t(k)}$$

The signal-to-interference-ratio (SIR) on the kth sub-carrier can be written as

$$SIR_k = \frac{E[|H_k P_t(k)|^2]}{E\left[\left|\sum_{n=0}^{m-1} \Phi_{k,n}^+(x_{0,n} - P_{t,n})\right|^2\right]} = \frac{|H_k|^2 |P_t(k)|^2}{\sum_{n=0}^{m-1} |\Phi_{k,n}^+|^2 E_s + \left|\sum_{n=0}^{m-1} \Phi_{k,n}^+ P_{t,n}\right|^2} \quad (49)$$

where E_s is the average energy of the data symbols. For $m < 0$, since the length of the channel delay spread spans L sampling periods, only $q = \max(L - (N_g + m), 0)$ block symbols are corrupted by the multipath components from the previous block. Assuming that there is a synchronization block preceding the CE block in a non-joint scheme and with the same transmitting power, it can be derived that the SIR is given by

$$SIR_k = \begin{cases} \frac{|H_k|^2 |P_t(k)|^2}{\sum_{n=0}^{q-1} |\Phi_{k,n}^-|^2 E_s + \left|\sum_{n=0}^{q-1} \Phi_{k,n}^- P_{t,p+n}\right|^2} & q = 0 \\ \frac{|H_k|^2 |P_t(k)|^2}{\sum_{n=0}^{q-1} |\Phi_{k,n}^-|^2 E_s + \left|\sum_{n=0}^{q-1} \Phi_{k,n}^- P_{t,p+n}\right|^2} & q > 0 \end{cases} \quad (50)$$

for $m < 0$ where $\Phi_{k,n}^- = \sum_{i=0}^n h_{L-n+i} e^{-j2\pi ik / N}$ and p

$= N - N_g - q$. It can be seen that timing error also affects the CE accuracy and will further degrade the system performance derived in Subsections FV-A and IV-B when the conventional preamble pattern is used.

V. Simulation Results and Discussions

MB-OFDM and SC-FDE block transmission schemes are for high-rate UWB systems. Thus, in the simulation, we set the block length $N = 128$, CP length $N_g = 32$, following [1]. This block length is determined based on practical implementation complexity. However, the resulting CP does not guarantee to be always longer than a UWB channel. The UWB channels simulated follow CM1-CM4 models proposed by the IEEE 802.15.3a Working Group [1]. A root raised cosine (RRC) pulse with a roll-off factor of 0.5 and span of [—

3T5,3T;] is used. Since the focus of this paper is timing synchronization, perfect carrier frequency synchronization is assumed in the simulation. The design parameters N_x and ℓ are determined according to the channel statistics. Fig. 5(a) gives the coarse timing error statistics, which shows the empirical cumulative distribution function (CDF) of the coarse timing error at $\hat{\gamma} = 10$ dB in CM1-CM4 UWB channels. It can be seen that the coarse timing error is most severe in CM4 which is the most dispersive channel model, indicating that the performance of the auto-correlation based coarse timing estimator is highly dependent on the channel condition. The more dispersive the channel is, the larger the coarse timing error. According to Fig. 5(a) we set $N_x = 30$. The choice of design parameter ℓ in the CTE estimator depends on the channel length statistics. If ℓ is too small, the estimation error probability is higher; Otherwise, the computation complexity is higher. We choose ℓ to be the average number of channel taps carrying 50% of the channel energy for different channel models. Fig. 5(b) shows the CDF of number of taps carrying 50% of the channel energy, using the channel sampling rate of 2 ns, and 1000 channel realizations for each channel model. It indicates that in CM4 ℓ can be chosen as 30, in CM3 $\ell = 25$, while in CM1 and CM2 $\ell = 15$ and $\ell = 20$ respectively.

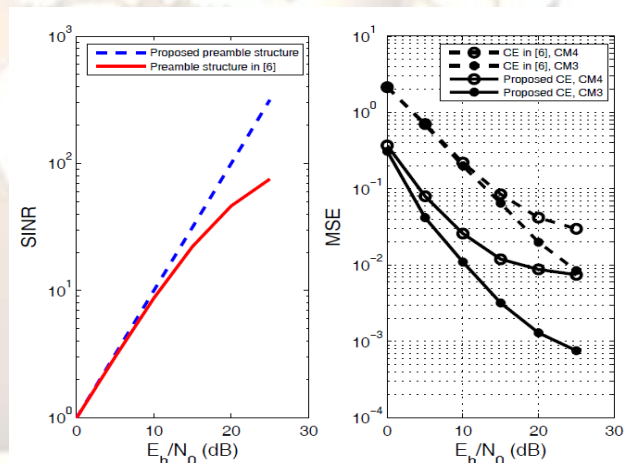


Fig. 10. (a) Average SINR of the coarse CE in CM1; (b) MSE performance of the channel estimator, with proposed preamble pattern and with the conventional preamble pattern.

The MAE performance shows that the proposed CE aided timing method outperforms conventional OFDM timing method significantly in UWB channels. The timing performance improvement of the proposed method over the conventional method comes from the more accurate coarse CE and the first tap searching algorithm. The proposed cyclic extended preamble structure can provide an IBI-free coarse stage CE regardless. For example, when the coarse timing position is on the right side of the true position, the coarse CE in [6]

will include samples of IBI. According to (49) in Section IV, the SIR of the coarse CE is given by

$$SIR_k + \frac{|H_k|^2 |P_t(k)|^2}{\sum_{n=0}^{\zeta-1} |\Phi_{k,n}^+(\zeta)|^2 E_s + |\sum_{n=0}^{\zeta-1} \Phi_{k,n}^+(\zeta) P_{t,n}|^2}$$

Where $\Phi_{k,n}^+(\zeta)$ is defined as in (47). The SINR results of the coarse CE obtained from simulation are plotted in Fig. 10(a) for the proposed scheme and that of [6] in CM1. In addition, the MSE performance of the channel estimator in CM3 and CM4 are compared in Fig. 10(b). Furthermore, the first tap searching algorithm in [6] is a conventional energy detector, whose performance is inferior to the proposed energy jump detector as described in Section III-C.

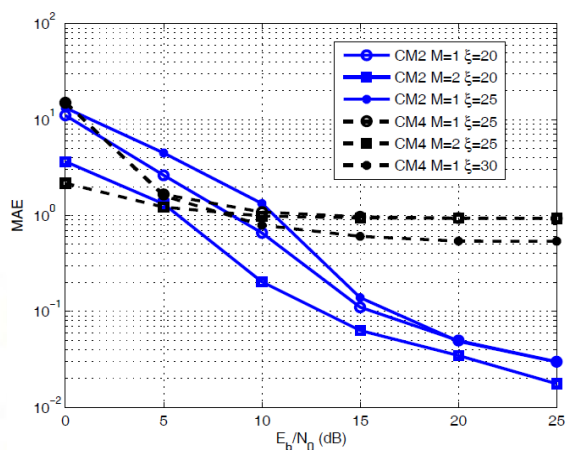


Fig. 11. MAE performance of the proposed scheme with different parameters.

Fig. 11 shows the timing performance with different design parameters, such as the number of repeated [A,B] (M) and ξ in the first tap search algorithm. It can be seen from Fig. 11 that in short channel conditions such as CMI or CM2, increasing ξ does not improve performance significantly, due to noise averaging (though not shown here), thus leading to better timing performance. However, increasing M in long channel conditions such as CM3 and CM4 cannot improve the performance at high SNRs whereas increasing ξ is more effective.

VI CONCLUSION

A joint timing and CE scheme that employs a unique preamble design and CIR assisted fine timing has been presented for UWB block transmission systems. The preamble proposed saves the overhead and has the cycle property resulting in CE and fine timing robust to coarse timing error. Based on the CE result, a novel algorithm for estimating the coarse timing error has been developed for UWB channels. Furthermore, the impact of symbol level timing error on an SC-FDE

system has been analyzed. Simulation results have shown that the proposed scheme yields accurate timing and superior CE performance in UWB channels.

REFERENCES

- [1] "Multi-band OFDM Physical Layer Proposal for IEEE 802.15 Task Group 3a," Mar. 2004.
- [2] Y. Wang and X. Dong, "Cyclic prefixed single carrier transmission in ultra-wideband communications," IEEE Trans. Wireless Commun., vol. 5, pp. 2017-2021, Aug. 2006.
- [3] "Comparison of frequency offset and timing offset effects on the performance of SC-FDE and OFDM over UWB channels," IEEE Trans. Veh. Technol., vol. 58, no. 1, pp. 242-250, Jan. 2009.
- [4] T. M. Schmidl and D. C. Cox, "Robust frequency and timing synchronization for OFDM," IEEE Trans. Commun., vol. 45, pp. 1613-1621, Dec. 1997.
- [5] M. Speth, F. Classen, and H. Meyr, "Frame synchronization of OFDM systems in frequency selective fading channels," in Proc. IEEE Veh. TechnoLConf., vol. 3, May 1997, pp. 1807-1811.
- [6] H. Minn, V. K. Bhargava, and K. B. Letaief, "A robust timing and frequency synchronization for OFDM systems," IEEE Trans. Wireless Commun., vol. 2, pp. 822-839, July 2003.
- [7] C. L. Wang and H. C. Wang, "An optimized joint time synchronization and channel estimation scheme for OFDM systems," in Proc. IEEE Veh. Technol. Conf., May 2008, pp. 908-912.
- [8] E. G. Larsson, G. Liu, J. Li, and G. B. Giannakis, "Joint symbol timing and channel estimation for OFDM based WLANs," IEEE Commun. Lett., vol. 5, no. 8, pp. 325-327, Aug. 2001.